Journal of Geoscience and Environment Protection, 2021, 9, 71-91
https://www.scirp.org/journal/gep
ISSN Online: 2327-4344
ISSN Print: 2327-4336

Morphological Profiles of Sand Dunes from ICESat-2 Geolocated Photons

Giribabu Dandabathula[1], Srinivasa Rao Sitiraju[1], Chandra Shekhar Jha[2]

[1]Regional Remote Sensing Centre-West, NRSC, Indian Space Research Organization, Jodhpur, India
[2]National Remote Sensing Centre, Indian Space Research Organization, Hyderabad, India
Email: dgb.isro@gmail.com, ssrao@nrsc.gov.in, jha_cs@nrsc.gov.in

How to cite this paper: Dandabathula, G., Sitiraju, S. R., & Jha, C. S. (2021). Morphological Profiles of Sand Dunes from ICESat-2 Geolocated Photons. *Journal of Geoscience and Environment Protection, 9,* 71-91.
https://doi.org/10.4236/gep.2021.92005

Received: January 12, 2021
Accepted: February 16, 2021
Published: February 19, 2021

Abstract

Aeolian process leads to the transportation and accumulation of sand particles that result in sand dune landforms. The structure and shape of the sand dunes are driven by the parameters of interacting wind force and the material composition of sand within. Cross-section profiles over the sand dunes will essay the geomorphological parameters through which the steady state and rate of sand transport can be computed. National Aeronautics and Space Administration's novel satellite namely Ice, Cloud and land Elevation Satellite-2 (ICESat-2) hosts a solo sensor namely Advanced Topographic Laser Altimeter System (ATLAS) which is a photon counting instrument that measures the round-trip time of the light pulse being emitted and reflected back from the surface determines the true height of the topographic feature on the Earth. In this article, cross-section profiles generated from the beams of ICESat-2 ground-tracks acquired over sand dunes of the Thar Desert region were analysed for detecting the geomorphological parameters. Observations from the cross-section profiles have resulted in giving unprecedented details about the shapes and morphological settings of various types of sand dunes like barchanoids, parabolic, longitudinal, and transverse dunes. Morphological parameters of sand dunes like the length of the stoss slope, crest height, slip face details, inter-arms spacing, height of the trailing arms, length of the depositional lobes, and sinuosity of the recurring crest lines were retrieved with ease from the Level-2A data product namely ATL03 of ICESat-2/ATLAS.

Keywords

Geomorphological Parameters, ICESat-2, Geolocated Photons, Sand Dunes, 2D Profiles

1. Introduction

Sand dunes occur in two distinct habitats; one on the barren waterless floors of

deserts and other along the coasts of seas and rivers (Bagnold, 1971). The steady state of sand dunes is controlled by the parameters of the agitating medium like wind vector (like velocity and direction) and the material composition of sand itself (Tsoar, 1985). Aeolian process leads to the transportation and accumulation of sand that result in sand dune formations that ranges from 1 meter to tens of kilometres in length and few tens of centimetres to over 300 meters the height (Bristow, 2009). Sand particles of various sizes will participate in the aeolian transport mechanism in several modes like saltation, reptation, and suspension (Bagnold, 1971; Kok et al., 2012). The shape of a sand dune depends entirely on sand deposit structure that gets influenced by the strength and direction of the interacting wind; as either transverse to the wind, longitudinal or lengthwise in the direction of the wind, or solitary dunes related to the varying wind direction (Edgell, 2006; Lorenz and Zimbelman, 2014).

Wasson and Hyde (1983) recognized four types of dunes based on wind regime and sand availability as barchans, transverse, longitudinal and star dunes; barchans occur where there are little sand and almost unidirectional winds, transverse dunes occur where sand is abundant and the wind is moderately variable, longitudinal dunes occur where the winds are more variable but there is little sand, and star dunes occur where sand is abundant and wind variability is at a maximum. Pye and Tsoar (1990) have considered the influence of vegetation (phytogenic) and further introduced parabolic dunes which have U or V shape with trailing arms. Cross-section profile analysis over sand dunes provides information regarding their shapes, heights, lengths, slopes and angle of repose of the structure. Tsoar (1985) while studying the steady state of sand dunes has emphasized the importance of cross-section profiles and appreciated its role in computing the rate of sand accumulation or sand loss. While utilizing the cross-section profiles over sand dunes, Zimbelman et al. (2012) have concluded that the profile information is a useful tool for evaluating possible mechanisms of the origin for aeolian-based features. In their studies, Courrech du Pont (2015) and Gao et al. (2015) have used the parameters from the cross-sections to study the dune morphodynamics and growth rates.

As most of the desert sand dunes are located in inaccessible regions, Earth observation systems help in providing a synoptic perspective to characterize the dune field patterns and boosted the understanding of arid zone geomorphology (Gutiérrez and Gutiérrez, 2013). Advances in remote sensing and spatial analysis have enabled better understanding of evolution, pattern development, morphometry and activity of sand dunes (Hugenholtz et al., 2012). Researchers have utilized remote sensing data to perform geomorphology studies over extra-terrestrial sand dunes (Radebaugh et al., 2010; Hayward et al., 2007; Al-Masrahy and Mountney, 2013; Bourke et al., 2010). Microwave remote sensing data has been used to retrieve geometrical characteristics of sand dunes (Stephan and Long, 2005) and to identify active/stabilized landforms in the driest deserts (Abdelkareem et al., 2020). Substantial advancements in the generation of Digital Elevation Models (DEM) and its availability to the scientific fraternity enabled research and reali-

zation of 3D aspects of sand dune geomorphology (Bubenzer and Bolten, 2008; Hugenholtz and Barchyn, 2010; Hugenholtz et al., 2012).

Advances in Light Detection And Ranging (LiDAR) data have expanded the possibilities to provide qualitative information about the morphological signatures and also enabled to monitor short term dune activities like volumetric changes (Hugenholtz et al., 2012). Satellite laser altimeter transmits laser pulses (energy in the order of several tens of mJ per pulse) towards target surfaces with a typical pulse rate of 10 - 30 Hz. The instrument measures the round-trip time of the light pulse between the emitted and the returned surface reflection to determine the distance of the spacecraft with respect to the surface and yields the true height of the topographic features on the ground (Falkner and Schulz, 2015). Space-based laser altimeters are effective in providing topographic measurements that are useful to understand the formation and early evolution of planetary bodies. Using laser altimetry data, geophysical parameters can be generated which provides significant insights related to the shape, structure, and evolution of the subject body (Cole, 1997). For subject areas like sand dunes, the surface measurements retrieved from consecutive orbits over a time period can be used to understand the morphological parameters and quantify the amount of sand transport. Integrating various remote sensing, photogrammetry and LiDAR are highly useful to monitor the changes in sand dune landforms.

1.1. Background to the ICESat Mission

National Aeronautics and Space Administration (NASA) has initiated space based laser altimeter mission namely Ice Cloud and Land Elevation Satellite (ICESat) that was designed to measure the changes on polar ice using on-board sensor titled Geoscience Laser Altimeter (GLAS) (Schutz et al., 2005). GLAS carried 532 nm (visible) and 1064 nm (near infrared) laser light to satisfy both atmospheric and topographic investigations. GLAS has operated by sending laser pulses at 40 Hz, and the transmitted laser pulse illuminates a spot on the Earth's surface with a diameter of 65 m and successive spots are separated on the Earth's surface by 172 m. The waveform data from GLAS contains transmitted time and echo received time that is used to compute the range measurements between the sensor platform and the Earth's surface (Martino et al., 2019). Measurements from the first ICESat satellite, which operated from 2003 to 2009 have provided vital information on the response of the Earth's frozen surface (Cryosphere) with respect to the changes of atmosphere and ocean parameters (Markus et al., 2017). ICESat mission has provided huge altimetry based measurements not only to the Cryosphere scientific community, but also to the ocean, terrestrial and atmospheric scientific communities. Potts et al. (2008) used ICESat data and a DEM from shuttle Radar Topography Mission (SRTM) for recognizing the seasonal dune changes in the Namib Desert. Dabboor et al. (2013) has successfully used ICESat laser altimetry data to track the sand dune migration in the Rub Al-Khali region. But, certain limitations with respect to its spatial resolutions

and single beam laser concept in the ICESat mission prohibited the full exploration of the data for scientific applications (Abdalati et al., 2010; Markus et al., 2017).

1.2. Photon Counting Sensor

ICESat-2 is a follow-up to the ICESat mission was launched in September 2018 and started releasing the data products with version 1 in May, 2019. ICESat-2 spacecraft carries a single instrument namely Advanced Topographic Laser Altimeter System (ATLAS) which sends pulses of laser light to the ground, collects the returning packets of energy called photons, and records the photon travel time (Blumenfeld, 2019). Photons of the trillion in number, starts the journey from ATLAS sensor, travelling through the atmosphere to reflect off the Earth's surface, return through the atmosphere and back into the ATLAS telescope. Of these, only few of the photons complete the journey and are recorded by on-board instruments (Markus et al., 2017). In comparison with the scientific concepts that was implemented in GLAS, ATLAS is entirely different in terms of pulse emitting process and spatial resolution; where ATLAS splits the laser pulse into six separate beams by a diffractive optical element, resulting in six individual footprints, each ~14 m in diameter arranged in the three pairs of beams. The 10 kHz laser repetition rate coupled with the ~500 km orbit produces along-track sampling interval of nearly 70 cm (0.7 m). The main application area of ICESat-2 is for cryosphere but extendable to measure elevations and detect the change in land forms, canopy, and water bodies (Abdalati et al., 2010; Neuenschwander and Pitts, 2019; Dandabathula et al., 2020). Initial assessment of height accuracy after evaluating the ICESat-2 data reported to detect centimeter level changes (Markus et al., 2017; Neuenschwander and Magruder, 2019; Kwok et al., 2019).

1.3. Objectives of the Study

A major objective of this study is to utilize the height information from the geolocated photon data obtained from the beams of ICESat-2 ground tracks acquired over various types of sand dunes; along-track sampled elevation is to be used to reconstruct the cross-section profiles to retrieve the geomorphological parameters pertaining to various sand dunes types. Towards this, samples of study areas falling in the Thar Desert region have been selected. Studies done on the sand dunes by earlier scholars in the Thar Desert region have been selected to infer and compare with the field level assessments.

Challenges exist to study sand dune morphology using optical remote sensing data and also photogrammetric techniques due to the homogeneous nature of sand dunes and shadows. The research in this article aims to bridge the gap due to the existing remote sensing techniques with the data from ICESat-2's along-track laser altimetry.

2. Materials and Methods

2.1. Study Area

The Thar Desert region is spread between the Aravalli hill ranges of India and

the Indus river of Pakistan, but its major presence is in Rajasthan state of India. The Thar Desert is dominated by aeolian landforms resulting in barchan, longitudinal, transverse, parabolic, dune complex, and dissected dune complex that occupies about 40 percent of the region (Kar, 2014).

Details about genesis, orientation, and distribution of sand dunes in the Thar Desert region were studied and reported by earlier scholars like Singh et al. (1972), Kar (1993), Kar (1996), Dhir and Singhvi (2012) and Wadhawan (2020). Kar (1996) has elaborated the morphological details of various active sand dunes in the Thar Desert region.

Breed et al. (1979) and Moharana et al. (2013) used satellite data to delineate and map various sand dune types in the Thar Desert region. In this study, six sample sites from the Thar Desert region were selected to analyse the cross-section profile from the ICESat-2 LiDAR data. The extents of these six sample sites were represented in **Figure 1**. The selection of these study areas was chosen so that

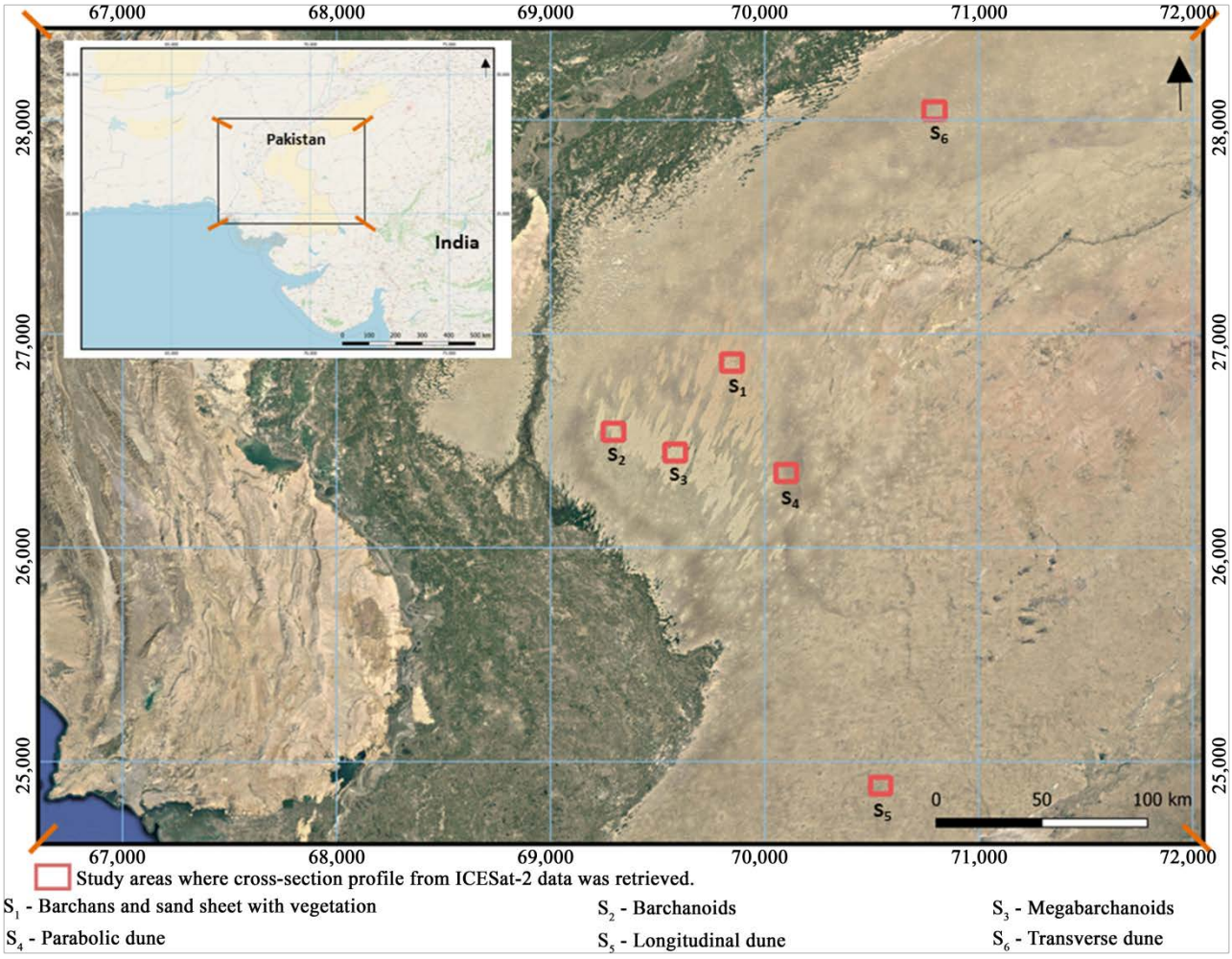

Figure 1. Map of the Thar Desert that spreads in India and Pakistan. The red colour rectangle boxes represent the selected sites that contain sand dunes of various types like barchanoids, megabarchanoids, parabola, linear, and traverse. These sites have been investigated for retrieving cross-sections from ICESat-2 LiDAR data. The satellite data in the main map is from Web Map Service (WMS) of Google Earth and inset of the image is from WMS of Open Street Map.

they contain major sand dunes types like barchanoids and sand sheets with vegetation (S1), barchanoids (S2), megabarchanoids (S3), parabolic (S4), longitudinal (S5), and transverse (S6).

2.2. Data Sets

The ICESat-2 Global Geolocated Photon Level-2A data product identified as ATL03 provides the latitude, longitude and ellipsoidal height of photons detected by the ATLAS instrument (Neumann et al., 2019b). The ATL03 product is used as the foundation for other surface-specific geophysical data products such as sea ice, land ice, and vegetation canopy height. All ICESat-2 data products are provided in the Hierarchical Data Format (HDF) and are available to the scientific fraternity from the web portal maintained by the National Snow and Ice Data Center (NSIDC—https://nsidc.org/data/icesat-2). Alternatively ICESat-2 data sets are available to visualize and download from the Geoportal titled OpenAltimetry (https://openaltimetry.org/). The footprint pattern formed by ICESat-2 laser beams contains six consecutive Ground Tracks (GT) that are defined from left to right in the direction of travel and termed as GT1L, GT1R, GT2L, GT2R, GT3L, and GT3R.

When ATLAS sensor makes forward orientation then these GTs contains the weak beams at the left side of the beam pair (GT1L, GT2L, and GT3L) and when the orientation is backwards then the relative positions of weak and strong beams changes. The ATL03 algorithm discriminates erroneous photon events and actual signal events; high confidence photons can be considered by setting the parameter "signal_conf_ph" to the value of 4 (Neumann et al., 2019a).

ATL03 data product undergoes numerous corrections with respect to solid earth tides, ocean loading, solid earth pole tide, ocean pole tide, and the wet and dry atmospheric delays; finally the data product contains height above the ellipsoid, time and geodetic latitude and longitude for individual photons (Neumann et al., 2020). In this study, selected ground tracks obtained over different sand dunes types have been used to generate the cross-section profiles. **Figure 2** represents the six ground tracks of ICESat-2 geolocated photons data overlaid on a sand dune system.

2.3. Methodology

Selected study areas contain barchanoids, megabarchanoids, parabolic, longitudinal, and transverse types of sand dunes; Level-2A data product titled ICESat-2 ATL03 photon elevation data acquired over these study areas were used to generate cross-section profiles for various sand dune types. Subsets of streams from ICESat-2 geolocated photons were converted into spatial format (GIS shape file) and overlaid on ortho-rectified high resolution data to study the individual sand dune type under the investigation. Cross sectiona profiles were drawn for the selected sand dunes. Each cross-section profile contains ellipsoidal height on y-axis, latitude on x-axis, date-time stamp of the ICESat-2 ground track, and the

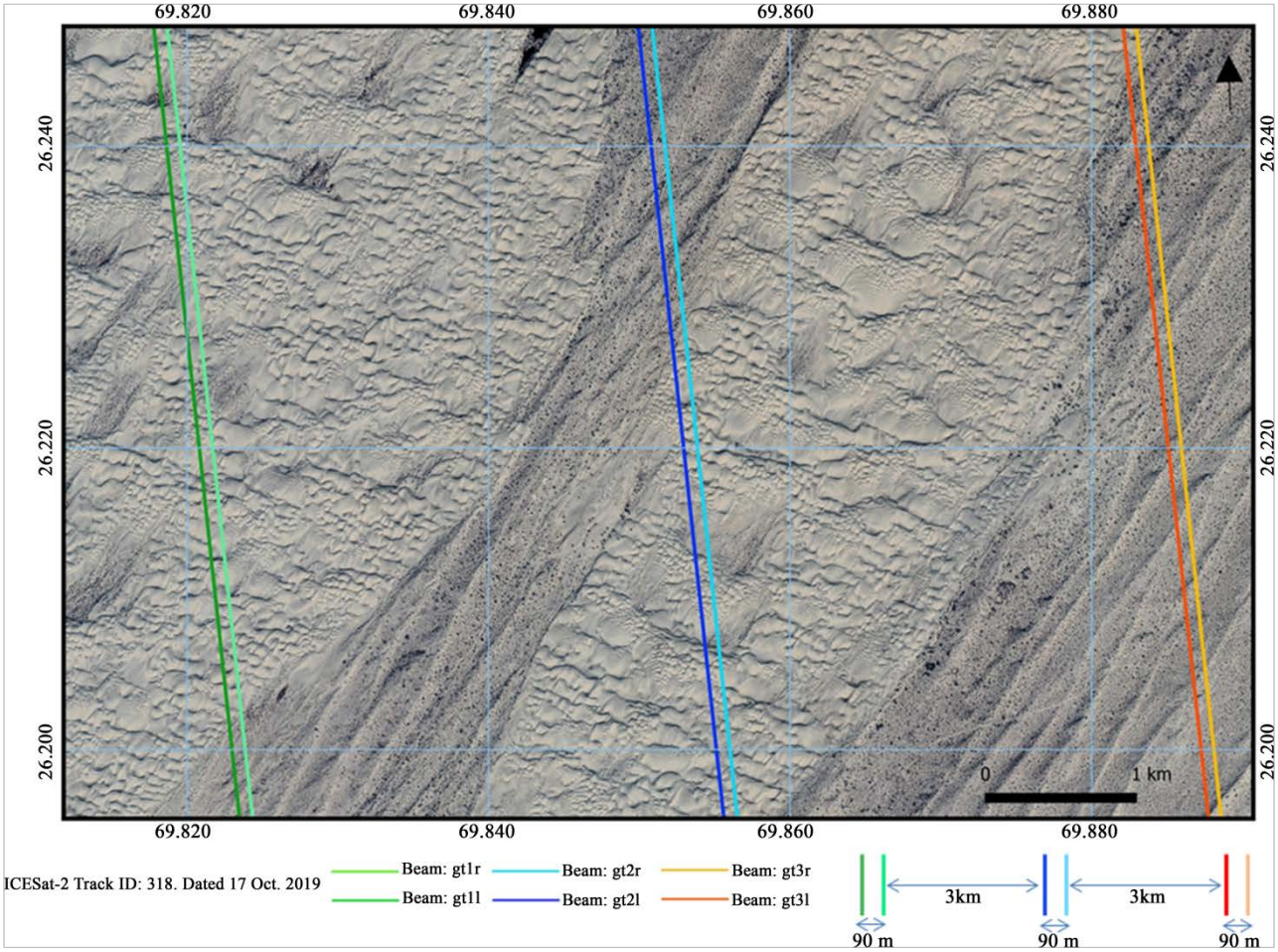

Figure 2. Illustration of 6 beams (3 pairs of strong and weak beams) from ICESat-2 ground track acquired over a sand dune system. Pair of tracks are approximately 3 km apart in the across-track direction and within each pair the weak and strong beams with an energy ration of approximately 1:4 are separated by 90 m in the across-track direction. The satellite image in the map is from Web Map Service of Google Earth.

beam details. Subsequent sections essays the observations from the cross-section analysis for all the six study sites belonging to this investigation.

3. Results and Discussion

ICESat-2 photon data has the ability to quantify canopy height and provides an indication of the vegetation structure (Neuenschwander and Magruder, 2019).

Sand sheets are planar and featureless surfaces with strata of continuous deposits of windblown fine-grained particles may be sparsely anchored with vegetation (Grotzinger et al., 2005; Lorenz and Zimbelman, 2014). Study area earmarked as S1 contains sand sheet with sparse vegetation and barchan chain of sand dunes. **Figure 3(a)** shows the high resolution satellite data from Web Map Service (WMS) of Google Earth overlaid with one beam of ICESat-2 photon data. **Figure 3(b)** shows the cross-section profile of the photon beam vector that was overlaid on the satellite image depicted in **Figure 3(a)**. A barchan chain or barchanoid ridge is an asymmetrical wavy dune ridge consisting of parallel rows

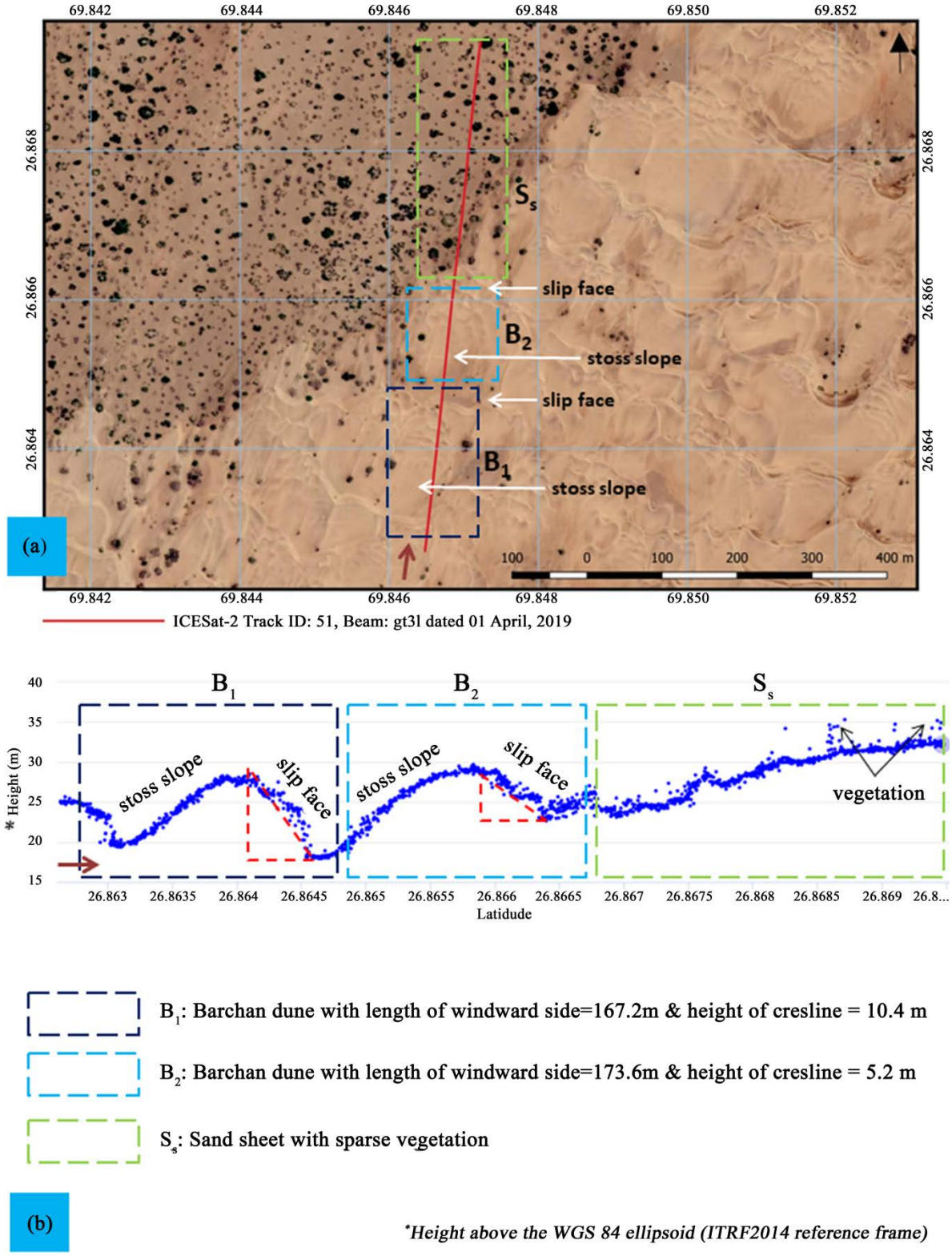

Figure 3. Cross-section profile generated from ICESat-2 photon counting data over an area containing barchan sand dunes and sand sheet with sparse vegetation. (a) High resolution satellite data from Web Map Service of Google Earth overlaid with ICESat-2's beam. The extent of the area contains sand sheet with sparse vegetation and barchanoids. (b) Cross-section profile for two barchan sand dunes and for sand sheet with sparse vegetation. Morphological parameters like length of the windward side and height of the slip face can be computed from the cross-section analysis.

of coalesced barchans (connected crescents) and is oriented transverse to the predominant wind direction and migrates forward (Tirsch, 2015). Solitaire barchans and barchanoids usually have gently dipping windward slopes and steeply dipping leeward slopes (slip face). From **Figure 3(b)**, it can be noted that the morphological parameters for the barchanoids (earmarked as B1 and B2) like length of the windward base and height of the slip face can be retrieved from the cross-section profiles. These morphological parameters play pivotal role while computing the rate of sand transport when using temporal data. The rate of barchan advance is directly related to the rate of sand transport over the brink and inversely related to the brink height (Pye and Tsoar, 1990; Haff and Presti, 1995; Ould Ahmedou et al., 2007). The cross-section profile for the sand sheet with sparse vegetation is also reconstructed in **Figure 3(b)**; gradual topographic relief for the sand sheets with signals from the vegetation is well represented in the profile.

Figure 4(a) shows the sample of the study area containing barchanoids. **Figure 4(b)** and **Figure 4(c)** show the cross-section profiles derived from the ICESat-2 weak beam and strong beam of a ground track respectively. It can be noted from **Figure 3(b)**, **Figure 4(b)**, and **Figure 4(c)**, the alternating elements of the consecutive barchans showing one downwind-facing barchanoid following by an upwind-facing linguoid element; the concept discussed earlier by researchers (Inman et al., 1966; Pye and Tsoar, 1990). Earlier researchers have done extensive field work and mapped the barchanoids in this study area and recorded their height range to be 10 to 15 m (Kar, 1993; Singhvi and Kar, 2004). The cross-section profiles retrieved from the ICESat-2 LiDAR data to confirm the height range of these barchanoids in these study area to be ranging between 10 to 15 m.

Compound dunes consist of two or more dunes of the same type combined by overlapping or being superimposed (McKee, 1979). Sample of the study area (earmarked as S3 in **Figure 1**) falling in the contiguous part of India and Pakistan contains compound barchanoids which were termed as megabarchanoids by Kar (1990) on the basis of their arrangement as tiers of barchanoids with significant height and size. The high resolution satellite image shown (part of study area S3) in **Figure 5(a)** shows the extent containing giant dunes with the tiers of barchans along their windward slopes that are arranged in a fish-scale pattern. The height of compound megabarchanoids ranges between 15 to 25 m and the height of fringing simple barchanoids on their windward slope are in the range of 1 to 5 m.

The noteworthy observation from the cross-section analysis is the ability to detect the length and height of the simple barchanoids located roughly from the lower mid-slip to the crestal segment of the windward base by the ICESat-2 LiDAR data. **Figure 5(b)** and **Figure 5(c)** illustrate the cross-section profiles retrieved form the pair of weak and strong beam (that are 90 m apart) of ICESat-2 ground track. The fish-scale patterns (earmarked with FS1, FS2, FS3, and FS4 in

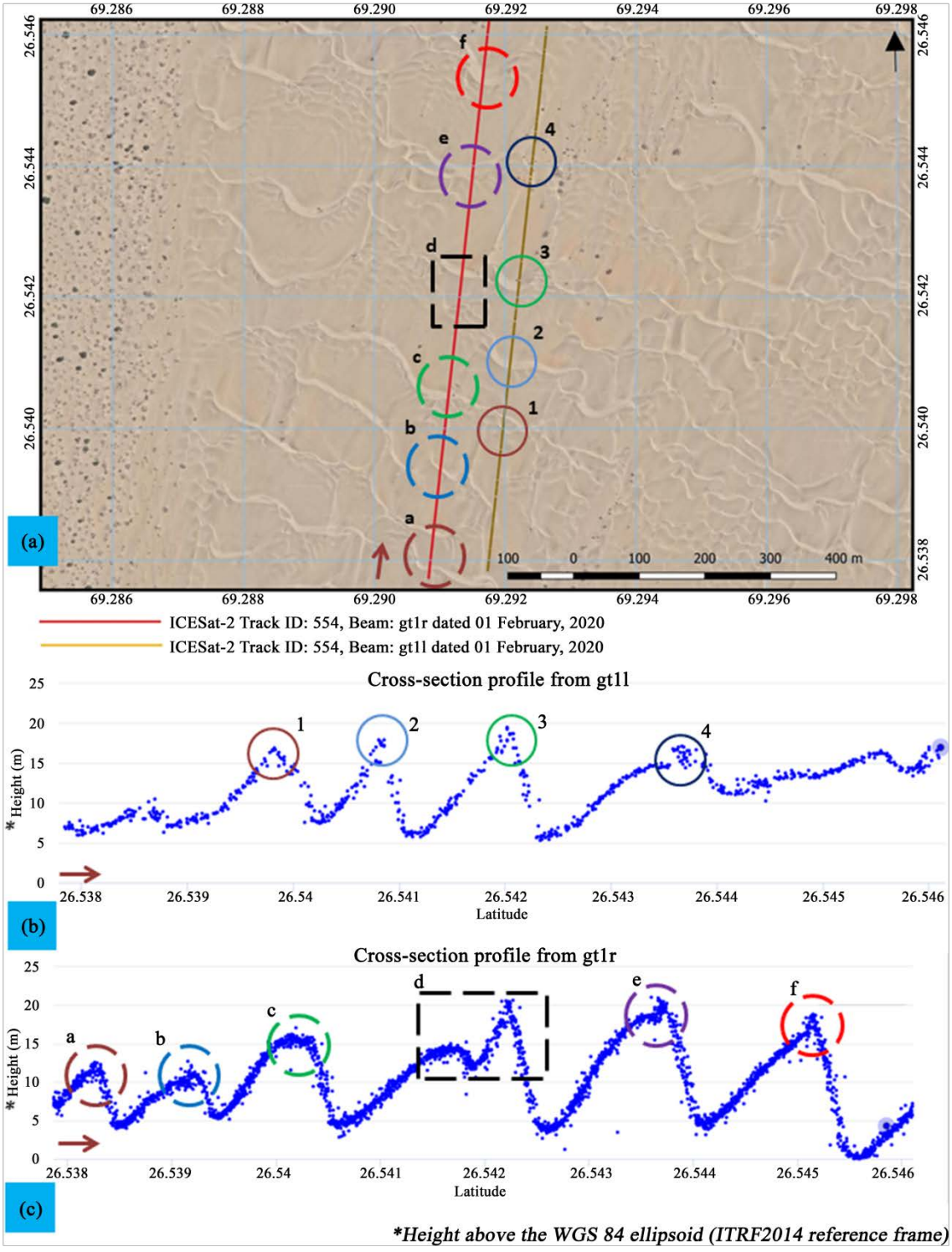

Figure 4. Cross-section profile generated from ICESat-2 photon counting data over an area containing barchanoid sand dunes. (a) High resolution satellite data from Web Map Service of Google Earth overlaid with pair of weak and strong beams from ICESat-2 LiDAR data. The extent of the area contains parallel rows of coalesced barchans. (b) Cross-section profile generated from weak beam of ICESat-2 LiDAR data over a sequence of barchanoids; Note the ridges of four barchanoids were highlighted with the colour circles. (c) Cross-section profile generated from strong beam of ICESat-2 LiDAR data over a sequence of barchanoids; Note the ridges of six barchanoids were highlighted with colour circles/box. Morphological parameters pertaining to the barchanoids like length of the windward side slip face can be computed from the cross-section analysis.

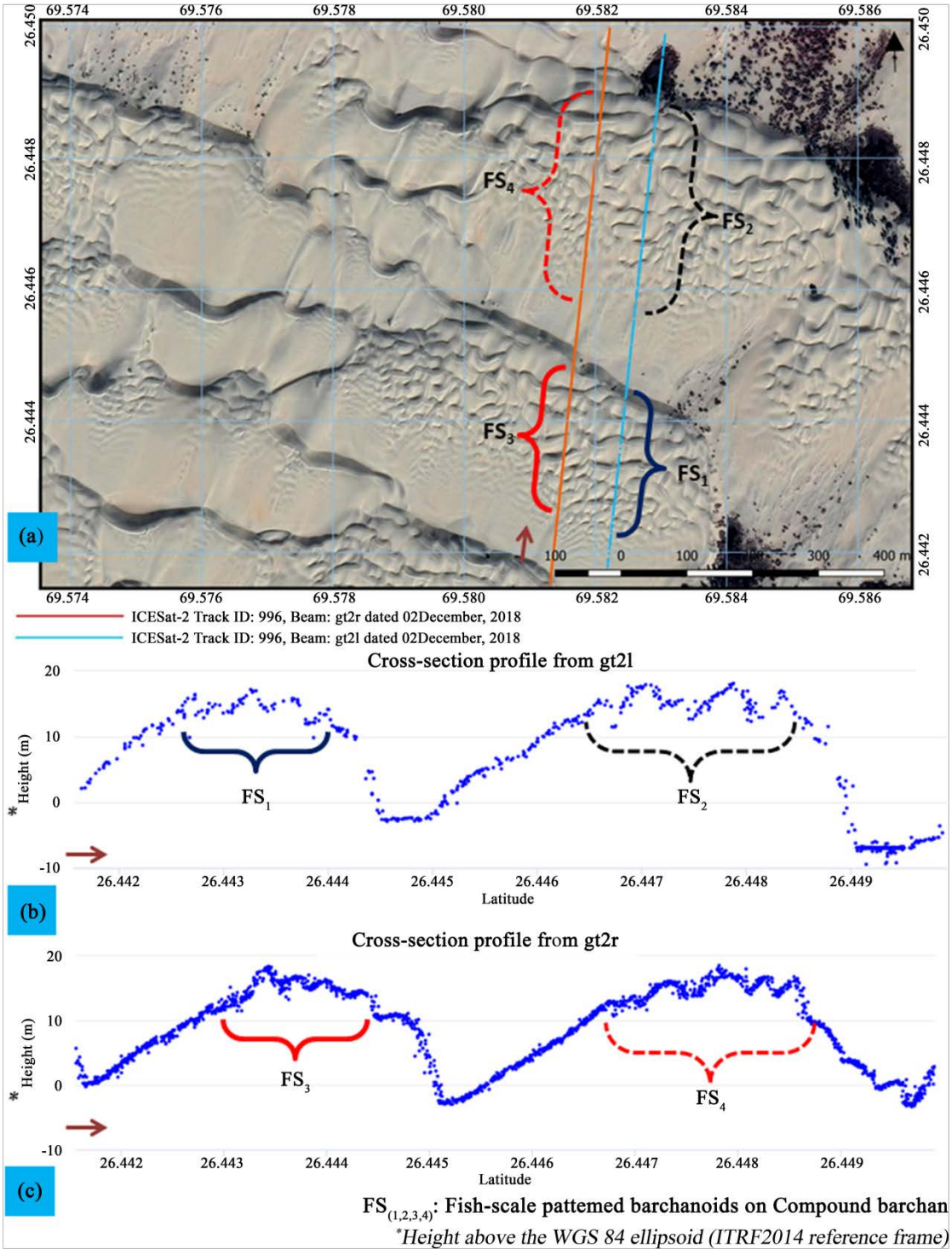

Figure 5. Cross-section profile generated from ICESat-2 photon counting data over an area containing compound barchanoid sand dunes. (a) High resolution satellite data from Web Map Service of Google Earth overlaid with pair of weak and strong beams from ICESat-2 LiDAR data. The extent of the area shown in the image map contains giant dunes with the tiers of barchans along their windward slopes that are arranged in a fish-scale pattern from the lower mid-slip to the crestal segment of the windward base. (b) Cross-section profile generated from weak beam of ICESat-2 LiDAR data over the compound barchanoid sand dunes. (c) Cross-section profile generated from strong beam of ICESat-2 LiDAR data over the compound barchanoid sand dune. Note the ridges of little barchan dunes which are present on the windward flanks with height ranging 1 to 5 m over the giant barchanoid dune of height ranging 15 to 20 m.

Figure 5(b) and **Figure 5(c)**) represent the minor barchanoids with height ranging 1 to 5 m over the compound barchanoids of height ranging 15 to 20 m. McKee (1979) has earlier discussed these type of compound dune types where little barchan dunes superimposed on the windward flanks of large ones and ICESat-2 LiDAR data enabled to detect these type of sand dunes with the geolocated photon data that will able to detect height changes in the order of centimetres.

Parabolic dunes are hairpin shaped (or tend to be U-shaped or V-shaped) landforms that have three basic features: a depositional lobe on the downwind side, trailing arms or ridges, and a deflation basin between the trailing arms (Goudie, 2011). **Figure 6(a)** shows the extent of typical parabolic dunes that exists in the Thar Desert region and the area under investigation (sample of study area earmarked as S4) to retrieve the cross-section profile from the ICESat-2 LiDAR data. **Figure 6(b)** and **Figure 6(c)** represent the cross-section profiles from the pair of weak and strong beams of ICESat-2 ground track. Parabolic dune arms are almost always stabilized by some form of vegetation (May, 2015) and are evident in **Figure 6(a)** where there is presence of sparse vegetation. Cross-section profiles generated over the parabolic dunes clearly highlights presence of the trailing arms or ridges (earmarked with +, ~, *, ~ and & in **Figure 6(b)** and **Figure 6(c)**). Earlier, scholars like Kar (1996) and Srivastava et al. (2019) explored this region and mentioned that the inter-arm spacing of these parabolic dunes ranges between 30 to 650 m of length, dunes in the middle of the parabolic cluster will be of longer arms, and presence of gradually shorter arms on each side of it; the same has been essayed by the cross-section profiles generated by ICESat-2 data which is being represented in **Figure 6(b)** and **Figure 6(c)**. In this sort of study area, the height of the ridges being in the range of 10 to 50 m and the same has been reported earlier by Kumar et al. (1993), Kar (1996), and Singhvi and Kar (2004). Cross-section profiles retrieved from ICESat-2 LiDAR data over parabolic dunes gives the dimensions of blowout hollow (deflation basin) through which basin morphology and wind flow patterns can be studied (Hesp, 2011).

Longitudinal dunes or linear dunes are elongated sand ridges of aeolian sediment forming approximately parallel to the resultant vector of long term prevailing wind direction (Radebaugh et al., 2015). Longitudinal dunes are also termed as seif dunes in Africa and Saudi Arabia. Details about the evolution of longitudinal dunes in the Thar Desert region were explored and reported by Kar (1993), Kumar et al. (1993), Wadhawan (1994), and Singhvi and Kar (2004). Kumar et al. (1993) attributed the reason for development of gullies in between the linear dunes is because of reactivation and break-down of a transverse sand ridge coalescing the trailing arms of the parabolic dunes through erosion by strong winds. In general, the length of longitudinal dunes is much greater than their width, and their long axes are parallel to the time-averaged vector sum of winds (Radebaugh et al., 2015). **Figure 7(a)** shows the extent of study area comprising

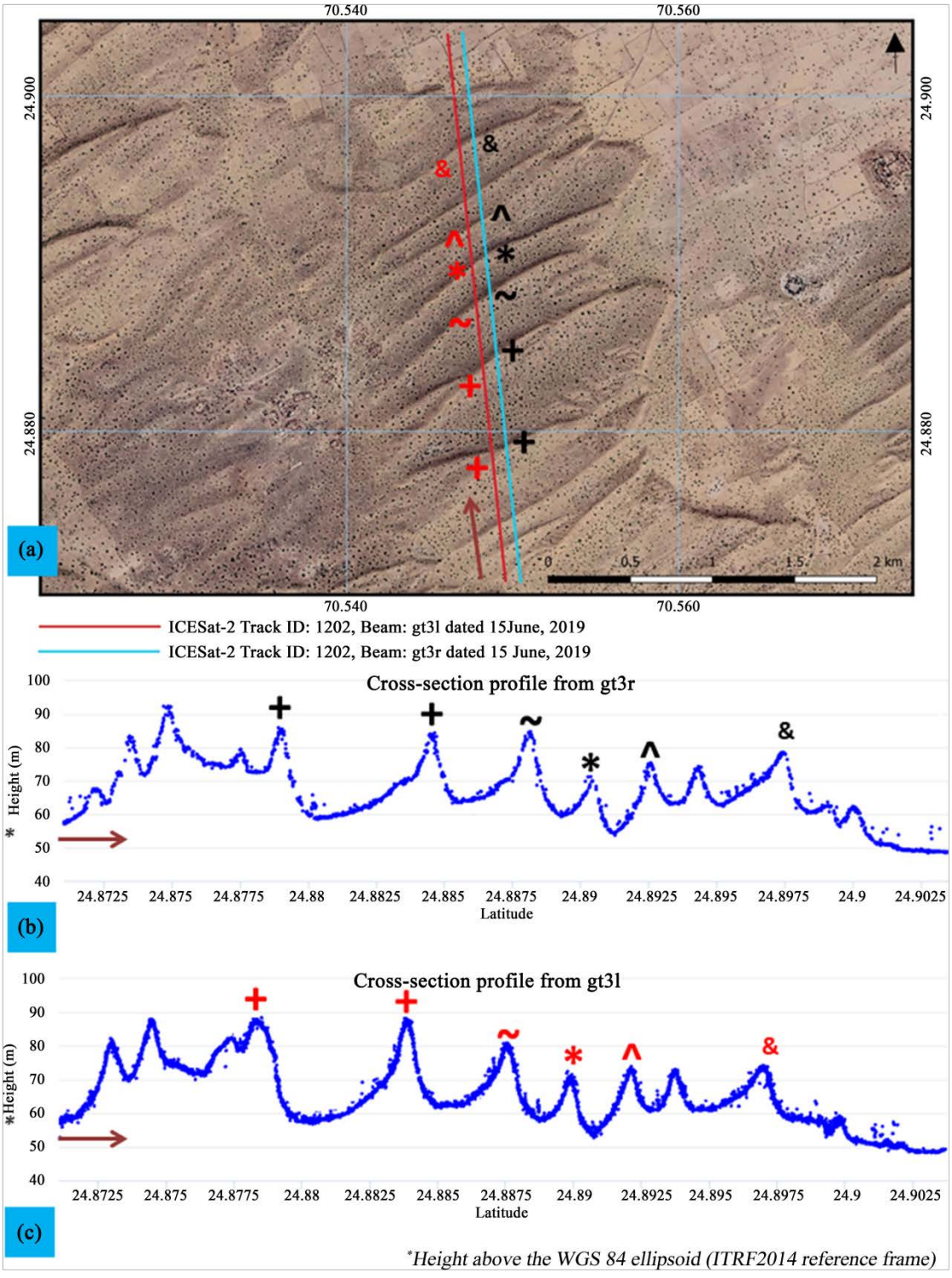

Figure 6. Cross-section profile generated from ICESat-2 photon counting data over an area containing parabolic sand dunes. (a) High resolution satellite data from Web Map Service of Google Earth overlaid with pair of weak and strong beams from ICESat-2 LiDAR data. The extent of the area shown in the image map contains parabolic dunes. Note the parabolic dune earmarked with "++" which is in the middle of cluster with longest arms in comparison with the parabolic dunes with shorter arms on either side (b) Cross-section profile generated from weak beam of ICESat-2 LiDAR data over the parabolic dunes. (c) Cross-section profile generated from strong beam of ICESat-2 LiDAR data over the parabolic dunes. Note the ridges formed by the trailing arms of the parabolic dunes.

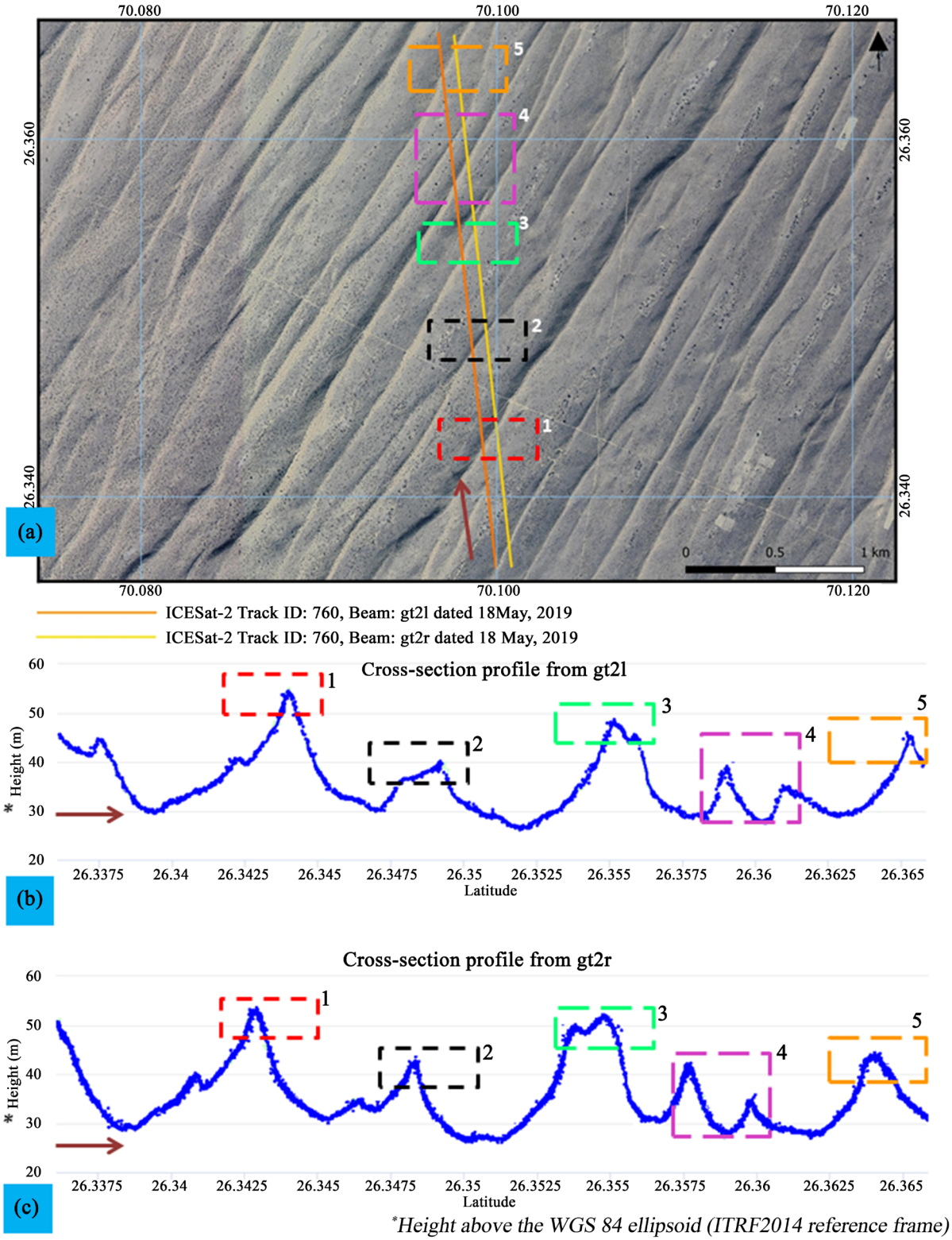

Figure 7. Cross-section profile generated from ICESat-2 photon counting data over an area containing longitudinal sand dunes. (a) High resolution satellite data from Web Map Service of Google Earth overlaid with pair of weak and strong beams from ICESat-2 LiDAR data. The extent of the area shown in the image map contains longitudinal dunes. (b) Cross-section profile generated from weak beam of ICESat-2 LiDAR data over a sequence of longitudinal dunes. (c) Cross-section profile generated from strong beam of ICESat-2 LiDAR data over a set of longitudinal dunes. Ridges of crest lines are indicated with the colour boxes.

the longitudinal dunes in the Thar Desert region (sample of study area earmarked as S5). **Figure 7(b)** and **Figure 7(c)** represent the cross-sectional profiles retrieved from ICESat-2 LiDAR data over the longitudinal dunes. Kar (1993) and Kumar et al. (1993) independently reported the height of the crest lines of these longitudinal dunes ranging from 5 to 50 m; through this study, similar dimensions have been retrieved form the ICESat-2 LiDAR data. The morphological parameters like height of crest lines, angle of linearity, and inter-spacing pattern between the crest lines can be used to deduce the wind regimes history and dune field state of development (Reffet et al., 2010). The pattern of slip faces occurring on either side of the dune long axis will give information about the recent winds regimes (Radebaugh et al., 2015).

Transverse dunes resemble barchan dunes in being a product of unidirectional winds, with steep slip faces oriented normal to wind direction and may occur in a gradational sequence (Fitzsimmons, 2015). Evolution details and structural parameters of transverse dunes have been reported by McKee (1979). Transverse dunes develop where sand is abundant and attain maximum height where there is a balance between strength of the wind and available sand (McKee, 1979; Kar, 1990; Tsoar and Blumberg, 2002). Multiple apices can form in the presence of adjacent dunes or landforms which influence wind orientation on a local scale (Bagnold, 1971). **Figure 8(a)** shows the transverse dunes located at the northern side of the Thar Desert (earmarked as a study area S6). **Figures 8(b)-(d)** show the cross-section profiles retrieved from ICESat-2 LiDAR data using three strong beams of ground tracks. Slip faces in the profiles have been highlighted with colour shapes. The profiles strongly give evidence of superimposed bedforms and crestline sinuosity. Crestline sinuosity represents the repetitive pattern of crests and Zhang et al. (2010) while modelling the transverse dune using cellular automata techniques mentioned that the crestline sinuosity is a useful parameter to determine the steady state of transverse dune. Kumar et al. (1993) in his report mentioned the occurrence of steep slip faces in this area; from the cross-section profile obtained from the ICESat-2 LiDAR the height of the certain slip faces ranges from 20 to 40 m indicating the steepness of the slip face. Kar (1996) in his research about this study area mentioned that the height of the crestlines for old dunes ranges from 20 to 40 m and there exists sub-parallel linear ribs along their windward slopes; **Figure 8(a)** shows the linear ribs and **Figure 8(d)** (between the dark and light green boxes) shows the linear ribs of height ranging 2 to 5 m.

4. Conclusion

Sand dunes are the geomorphological records of the aeolian processes and their shapes represent the wind regime and history of sand transport. Profiles from space based laser altimeters like ICESat-2 are effective in providing the topographic measurements and profiling the landform shapes. In this article, samples of sand dunes located in the Thar Desert region have been studied using geolocated photons from ICESat-2 data. Cross-section profiles generated from various

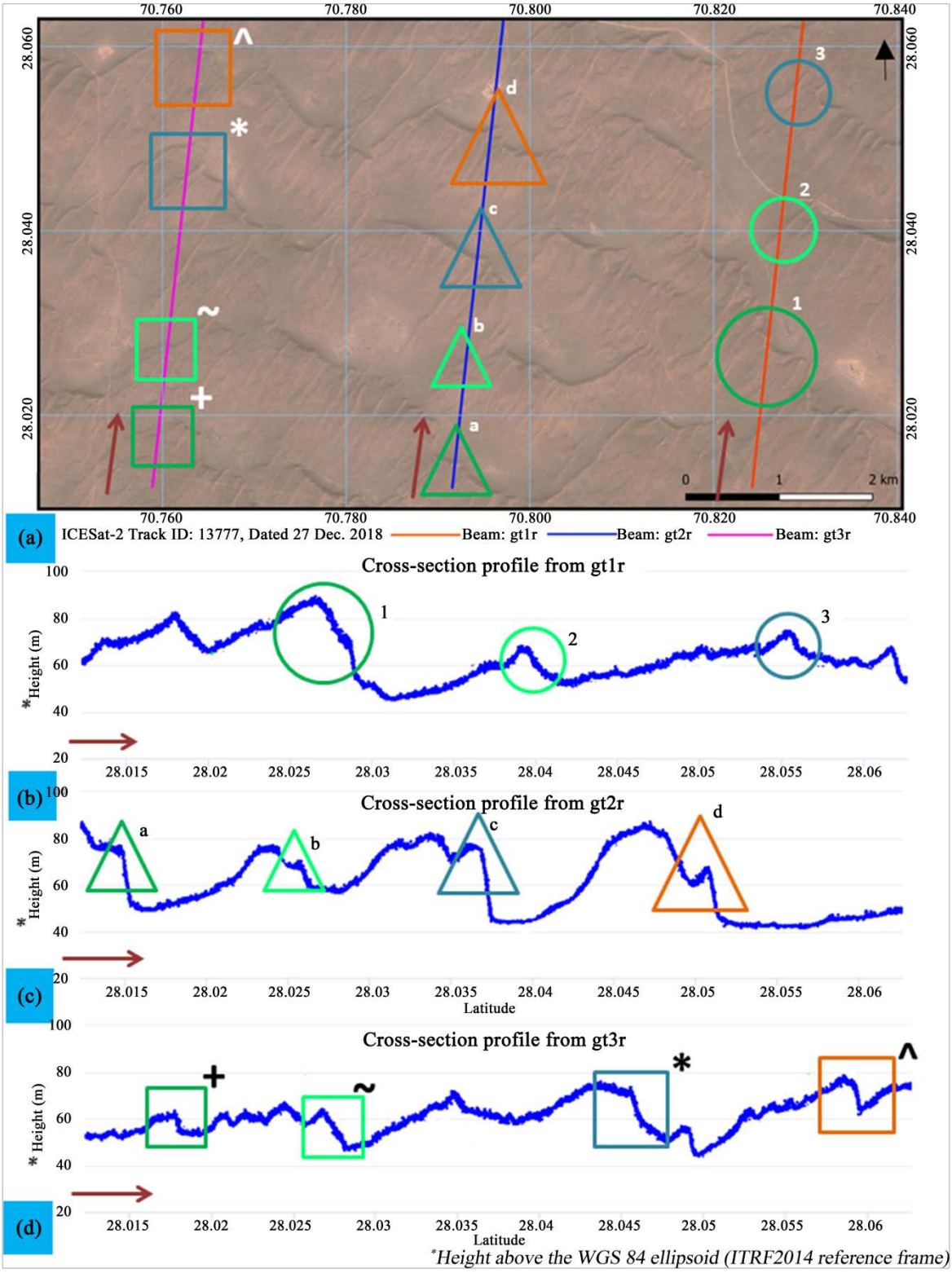

Figure 8. Cross-section profile generated from ICESat-2 photon counting data over an area containing transverse sand dunes. (a) High resolution satellite data from Web Map Service of Google Earth overlaid with three strong beams from ICESat-2 LiDAR data. The extent of the area shown in the image map contains transverse dunes. (b)-(d) Cross-section profile generated from strong beams of ICESat-2 LiDAR data over a bed of transverse dunes. Ridges of crest lines are indicated with the colour boxes/triangles/circles.

beams of the ICESat-2 ground tracks have shown that the ability to distinguish between sand sheets and sand dunes in the semi-arid regions. Morphological parameters of the sand dunes like the length of the windward side, height of slip face, and crestline can be retrieved from the cross-section profiles generated from the photon elevation data of ICESat-2 due to its ability to generate dense along-track sampling (~ 70 cm). Importantly, ICESat-2 will give the elevation estimates over high sloped area and thus, mensuration over features like slip face will enable us a better understanding of the sand dune structures. Also, studying the distances between the crests of successive barchanoids (wavelength) is useful to quantify the saltation. High sampling feature of ICESat-2 photon events with centimeter level accuracies are able to fetch the details of minor elevations carved by the superimposed features on the main structure in compound dunes. Structural details like distance between inter-arm spacing, height of the trailing arms, shape of deflation basin, and pattern of slip faces can be retrieved using cross-section profiles for parabolic and longitudinal sand dunes. Unprecedented details about the shapes and morphological settings of the sand dunes have been reported through the cross-section profiles generated from the ICESat-2 photon data.

Future work can include the integration of ICESat-2 data with optical remote sensing data for automatic recognizing of sand dunes. However, limitation in the study is the availability of the cross-section profile direction that restricts to study landform of the sand dune in its entire form.

Acknowledgements

We thank Director, National Remote Sensing Centre for facilitating the institutional support and for providing basic infrastructure for this investigation. We thank Dr. B.K Bhadra and all officials of RRSC-West, NRSC/ISRO, Jodhpur for providing constructive ideas related to this research. The authors would like to mention a special thanks to Mr. Rajkumar Seet for providing valuable insights in this research.

Conflicts of Interest

The authors declare no conflicts of interest regarding the publication of this paper.

References

Abdalati, W., Zwally, H. J., Bindschadler, R., Csatho, B., Farrell, S. L., Fricker, H. A., Harding, D., Kwok, R., Lefsky, M., Markus, T., Marshak, A., Neumann, T., Palm, S., Schutz, B., Smith, B., Spinhirne, J., & Webb, C. (2010). The ICESat-2 Laser Altimetry Mission. *Proceedings of the IEEE, 98,* 735-751. https://doi.org/10.1109/JPROC.2009.2034765

Abdelkareem, M., Gaber, A., Abdalla, F., & El-Din, G. K. (2020). Use of Optical and Radar Remote Sensing Satellites for Identifying and Monitoring Active/Inactive Landforms in the Driest Desert in Saudi Arabia. *Geomorphology, 362,* Article ID: 107197. https://doi.org/10.1016/j.geomorph.2020.107197

Al-Masrahy, M. A., & Mountney, N. P. (2013). Remote Sensing of Spatial Variability in Aeolian Dune and Interdune Morphology in the Rub' Al-Khali, Saudi Arabia. *Aeolian Research, 11,* 155-170. https://doi.org/10.1016/j.aeolia.2013.06.004

Bagnold, R. A. (1971). *The Physics of Blown Sand and Desert Dunes*. Berlin: Springer. https://doi.org/10.1007/978-94-009-5682-7

Blumenfeld, J. (2019). *ICESAT-2 Data Usher in a New Age of Exploration*. Tools and Technology Articles, EarthData, NASA. https://earthdata.nasa.gov/learn/articles/tools-and-technology-articles/icesat-2-data

Bourke, M. C., Lancaster, N., Fenton, L. K., Parteli, E. J. R., Zimbelman, J. R., & Radebaugh, J. (2010). Extraterrestrial Dunes: An Introduction to the Special Issue on Planetary Dune Systems. *Geomorphology, 121,* 1-14. https://doi.org/10.1016/j.geomorph.2010.04.007

Breed, C. S., Fryberger, S. G., Andrews, S., McCauley, C., Lennartz, F., Gebel, D., & Horstman, K. (1979). Regional Studies of Sand Seas Using Landsat (ERTS) Imagery. In *A Study of Global Sand Seas* (pp. 305-397). Professional Paper No. 1052, Reston, VA: US Geological Survey.

Bristow, C. (2009). Ground Penetrating Radar in Aeolian Dune Sands. In *Ground Penetrating Radar Theory and Applications* (pp. 271-297). Amsterdam: Elsevier. https://doi.org/10.1016/B978-0-444-53348-7.00009-0

Bubenzer, O., & Bolten, A. (2008). The Use of New Elevation Data (SRTM/ASTER) for the Detection and Morphometric Quantification of Pleistocene Megadunes (DRAA) in the Eastern Sahara and the Southern Namib. *Geomorphology, 102,* 221-231. https://doi.org/10.1016/j.geomorph.2008.05.003

Cole, T. D. (1997). Spaceborne Laser Altimetry. *Advancement of Photonics for Space: A Critical Review,* Volume 10288, 102880G. https://doi.org/10.1117/12.278755

Courrech du Pont, S. (2015). Dune Morphodynamics. *Comptes Rendus Physique, 16,* 118-138. https://doi.org/10.1016/j.crhy.2015.02.002

Dabboor, M. D., Braun, A., & Kneen, M. A. (2013). Tracking Sand Dune Migration in the Rub Al-Khali with ICESat Laser Altimetry. *International Journal of Remote Sensing, 34,* 3832-3847. https://doi.org/10.1080/01431161.2012.762483

Dandabathula, G., Verma, M., Satyanarayana, P., & Srinivasa Rao, S. (2020). Evaluation of ICESat-2 ATL08 Data Product: Performance Assessment in Inland Water. *European Journal of Environment and Earth Sciences, 1,* 1. https://doi.org/10.24018/ejgeo.2020.1.3.15

Dhir, R. P., & Singhvi, A. K. (2012). The Thar Desert and Its Antiquity. *Current Science, 102,* 1001-1008. http://www.jstor.org/stable/24084539

Edgell, H. S. (2006). *Arabian Deserts: Nature, Origin and Evolution*. Berlin: Springer Science & Business Media. https://doi.org/10.1007/1-4020-3970-0

Falkner, P., & Schulz, R. (2015). Instrumentation for Planetary Exploration Missions. In *Treatise on Geophysics* (pp. 719-755). Amsterdam: Elsevier. https://doi.org/10.1016/B978-0-444-53802-4.00181-0

Fitzsimmons, K. E. (2015). Transverse Dunes. In *Encyclopedia of Planetary Landforms* (pp. 2185-2187). New York: Springer. https://doi.org/10.1007/978-1-4614-3134-3_381

Gao, X., Narteau, C., Rozier, O., & du Pont, S. C. (2015). Phase Diagrams of Dune Shape and Orientation Depending on Sand Availability. *Scientific Reports, 5,* Article No. 14677. https://doi.org/10.1038/srep14677

Goudie, A. (2011). Parabolic Dunes: Distribution, Form, Morphology and Change. *Annals of Arid Zone, 50,* 1-7.

Grotzinger, J. P., Arvidson, R. E., Bell, J. F., Calvin, W., Clark, B. C., Fike, D. A., Golombek, M., Greeley, R., Haldemann, A., Herkenhoff, K. E., Jolliff, B. L., Knoll, A. H., Malin, M., McLennan, S. M., Parker, T., Soderblom, L., Sohl-Dickstein, J. N., Squyres, S. W., Tosca, N. J., & Watters, W. A. (2005). Stratigraphy and Sedimentology of a Dry to Wet Eolian Depositional System, Burns Formation, Meridiani Planum, Mars. *Earth and Planetary Science Letters, 240,* 11-72. https://doi.org/10.1016/j.epsl.2005.09.039

Gutiérrez, M., & Gutiérrez, F. (2013). 13.8 Climatic Geomorphology. In *Treatise on Geomorphology* (pp. 115-131). Amsterdam: Elsevier. https://doi.org/10.1016/B978-0-12-374739-6.00346-8

Haff, P. K., & Presti, D. E. (1995). Barchan Dunes of the Salton Sea Region, California. In *Desert Aeolian Processes* (pp. 153-177). Berlin: Springer. https://doi.org/10.1007/978-94-009-0067-7_7

Hayward, R. K., Mullins, K. F., Fenton, L. K., Hare, T. M., Titus, T. N., Bourke, M. C., Colaprete, A., & Christensen, P. R. (2007). Mars Global Digital Dune Database and Initial Science Results. *Journal of Geophysical Research, 112,* E11007. https://doi.org/10.1029/2007JE002943

Hesp, P. (2011). Dune Coasts. In *Treatise on Estuarine and Coastal Science* (pp. 193-221). Amsterdam: Elsevier. https://doi.org/10.1016/B978-0-12-374711-2.00310-7

Hugenholtz, C. H., & Barchyn, T. E. (2010). Spatial Analysis of Sand Dunes with a New Global Topographic Dataset: New Approaches and Opportunities. *Earth Surface Processes and Landforms, 35,* 986-992. https://doi.org/10.1002/esp.2013

Hugenholtz, C. H., Levin, N., Barchyn, T. E., & Baddock, M. C. (2012). Remote Sensing and Spatial Analysis of Aeolian Sand Dunes: A Review and Outlook. *Earth-Science Reviews, 111,* 319-334. https://doi.org/10.1016/j.earscirev.2011.11.006

Inman, D. L., Ewing, G. C., & Corliss, J. B. (1966). Coastal Sand Dunes of Guerrero Negro, Baja California, Mexico. *Geological Society of America Bulletin, 77,* 787-802. https://doi.org/10.1130/0016-7606(1966)77[787:CSDOGN]2.0.CO;2

Kar, A. (1990). Megabarchanoids of the Thar: Their Environment, Morphology and Relationship with Longitudinal Dunes. *The Geographical Journal, 156,* 51. https://doi.org/10.2307/635436

Kar, A. (1993). Aeolian Processes and Bedforms in the Thar Desert. *Journal of Arid Environments, 25,* 83-96. https://doi.org/10.1006/jare.1993.1044

Kar, A. (1996). Morphology and Evolution of Sand Dunes in the Thar Desert as Key to Sand Control Measures. *Indian Journal of Geomorphology, 1,* 177-206.

Kar, A. (2014). The Thar or the Great Indian Sand Desert. In *World Geomorphological Landscapes* (pp. 79-90). Berlin: Springer. https://doi.org/10.1007/978-94-017-8029-2_7

Kok, J. F., Parteli, E. J. R., Michaels, T. I., & Karam, D. B. (2012). The Physics of Wind-Blown Sand and Dust. *Reports on Progress in Physics, 75,* Article ID: 106901. https://doi.org/10.1088/0034-4885/75/10/106901

Kumar, M., Goossens, E., & Goossens, R. (1993). Assessment of Sand Dune Change Detection in Rajasthan (Thar) Desert, India. *International Journal of Remote Sensing, 14,* 1689-1703. https://doi.org/10.1080/01431169308953995

Kwok, R., Markus, T., Kurtz, N. T., Petty, A. A., Neumann, T. A., Farrell, S. L., Cunningham, G. F., Hancock, D. W., Ivanoff, A., & Wimert, J. T. (2019). Surface Height and Sea Ice Freeboard of the Arctic Ocean from ICESat-2: Characteristics and Early Results. *Journal of Geophysical Research: Oceans, 124,* 6942-6959. https://doi.org/10.1029/2019JC015486

Lorenz, R. D., & Zimbelman, J. R. (2014). Sand. In *Dune Worlds* (pp. 17-25). Berlin: Springer. https://doi.org/10.1007/978-3-540-89725-5_2

Markus, T., Neumann, T., Martino, A., Abdalati, W., Brunt, K., Csatho, B., Farrell, S., Fricker, H., Gardner, A., Harding, D., Jasinski, M., Kwok, R., Magruder, L., Lubin, D., Luthcke, S., Morison, J., Nelson, R., Neuenschwander, A., Palm, S., Zwally, J. et al. (2017). The Ice, Cloud, and Land Elevation Satellite-2 (ICESat-2): Science Requirements, Concept, and Implementation. *Remote Sensing of Environment, 190,* 260-273. https://doi.org/10.1016/j.rse.2016.12.029

Martino, A. J., Neumann, T. A., Kurtz, N. T., & McLennan, D. (2019). ICESat-2 Mission Overview and Early Performance. *Sensors, Systems, and Next-Generation Satellites XXIII,* Strasbourg, 9-12 September 2019, 111510C. https://doi.org/10.1117/12.2534938

May, J. H. (2015). Parabolic Dune. In *Encyclopedia of Planetary Landforms* (pp. 1515-1518). New York: Springer. https://doi.org/10.1007/978-1-4614-3134-3_251

McKee, E. D. (1979). *A Study of Global Sand Seas*. Professional Paper, Reston, VA: US Geological Survey. https://doi.org/10.3133/pp1052

Moharana, P. C., Gaur, M. C., Choudhary, C., Chauhan, J. S., & Rajpurohit, R. S. (2013). A System of Geomorphological Mapping for Western Rajasthan with Relevance for Agricultural Land Use. *Annals of Arid Zone, 52,* 163-180.

Neuenschwander, A., & Pitts, K. (2019). The ATL08 Land and Vegetation Product for the ICESat-2 Mission. *Remote Sensing of Environment, 221,* 247-259. https://doi.org/10.1016/j.rse.2018.11.005

Neuenschwander, A. L., & Magruder, L. A. (2019). Canopy and Terrain Height Retrievals with ICESat-2: A First Look. *Remote Sensing, 11,* 1721. https://doi.org/10.3390/rs11141721

Neumann, T. A., Martino, A. J., Markus, T., Bae, S., Bock, M. R., Brenner, A. C., Brunt, K. M., Cavanaugh, J., Fernandes, S. T., Hancock, D. W., Harbeck, K., Lee, J., Kurtz, N. T., Luers, P. J., Luthcke, S. B., Magruder, L., Pennington, T. A., Ramos-Izquierdo, L., Rebold, T., Thomas, T. C. et al. (2019a). The Ice, Cloud, and Land Elevation Satellite-2 Mission: A Global Geolocated Photon Product Derived from the Advanced Topographic Laser Altimeter System. *Remote Sensing of Environment, 233,* Article ID: 111325. https://doi.org/10.1016/j.rse.2019.111325

Neumann, T., Brenner, A., Hancock, D., Robbins, J., Saba, J., Harbeck, K., & Gibbons, A. (2019b). *Ice, Cloud, and Land Elevation Satellite-2 (ICESat-2) Project: Algorithm Theoretical Basis Document (ATBD) for Global Geolocated Photons (ATL03)*. Washington DC: National Aeronautics and Space Administration, Goddard Space Flight Center.

Neumann, T. A., Brenner, A., Hancock, D., Robbins, J., Luthcke, S. B., Harbeck, K., Lee, J., Gibbons, A., Saba, J., & Brunt, K. (2020). *ATLAS/ICESat-2 L2A Global Geolocated Photon Data, Version 3 [Data Set]*. Washington DC: NASA National Snow and Ice Data Center DAAC.

Ould Ahmedou, D., Ould Mahfoudh, A., Dupont, P., Ould El Moctar, A., Valance, A., & Rasmussen, K. R. (2007). Barchan Dune Mobility in Mauritania Related to Dune and Interdune Sand Fluxes. *Journal of Geophysical Research, 112,* F02016. https://doi.org/10.1029/2006JF000500

Potts, L. V., Akyilmaz, O., Braun, A., & Shum, C. K. (2008). Multi-Resolution Dune Morphology Using Shuttle Radar Topography Mission (SRTM) and Dune Mobility from Fuzzy Inference Systems Using SRTM and Altimetric Data. *International Journal of Remote Sensing, 29,* 2879-2901. https://doi.org/10.1080/01431160701408352

Pye, K., & Tsoar, H. (1990). *Aeolian Sand and Sand Dunes*. Berlin: Springer. https://doi.org/10.1007/978-94-011-5986-9

Radebaugh, J., Lorenz, R., Farr, T., Paillou, P., Savage, C., & Spencer, C. (2010). Linear Dunes on Titan and Earth: Initial Remote Sensing Comparisons. *Geomorphology, 121,* 122-132. https://doi.org/10.1016/j.geomorph.2009.02.022

Radebaugh, J., Sharma, P., Korteniemi, J., & Fitzsimmons, K. E. (2015). Longitudinal Dunes (or Linear Dunes). In *Encyclopedia of Planetary Landforms* (pp. 1263-1271). New York: Springer. https://doi.org/10.1007/978-1-4614-3134-3_460

Reffet, E., Courrech du Pont, S., Hersen, P., & Douady, S. (2010). Formation and Stability of Transverse and Longitudinal Sand Dunes. *Geology, 38,* 491-494. https://doi.org/10.1130/G30894.1

Schutz, B. E., Zwally, H. J., Shuman, C. A., Hancock, D., & DiMarzio, J. P. (2005). Overview of the ICESat Mission. *Geophysical Research Letters, 32,* L21S01. https://doi.org/10.1029/2005GL024009

Singh, S., Ghose, B., & Vats, P. C. (1972). *Genesis, Orientation, and Distribution of Sand Dunes in Arid and Semi-Arid Regions of India.* Jodhpur: Central Arid Zone Research Institute.

Singhvi, A. K., & Kar, A. (2004). The Aeolian Sedimentation Record of the Thar Desert. *Journal of Earth System Science, 113,* 371-401. https://doi.org/10.1007/BF02716733

Srivastava, A., Thomas, D. S. G., & Durcan, J. A. (2019). Holocene Dune Activity in the Thar Desert, India. *Earth Surface Processes and Landforms, 44,* 1407-1418. https://doi.org/10.1002/esp.4583

Stephan, H., & Long, D. G. (2005). Modeling Microwave Emissions of Erg Surfaces in the Sahara Desert. *IEEE Transactions on Geoscience and Remote Sensing, 43,* 2822-2830. https://doi.org/10.1109/TGRS.2005.857899

Tirsch, D. (2015). Barchanoid Ridge. In *Encyclopedia of Planetary Landforms* (pp. 134-137). New York: Springer. https://doi.org/10.1007/978-1-4614-3134-3_13

Tsoar, H., & Blumberg, D. G. (2002). Formation of Parabolic Dunes from Barchan and Transverse Dunes along Israel's Mediterranean Coast. *Earth Surface Processes and Landforms, 27,* 1147-1161. https://doi.org/10.1002/esp.417

Tsoar, H. (1985). Profiles Analysis of Sand Dunes and Their Steady State Signification. *Geografiska Annaler: Series A, Physical Geography, 67,* 47-59. https://doi.org/10.1080/04353676.1985.11880129

Wadhawan, S. K. (1994). Dune Dynamics and Evolution of Aeolian Landforms in Parts of Jaisalmer District, Rajasthan, India. *Journal of the Indian Society of Remote Sensing, 22,* 65-77. https://doi.org/10.1007/BF03023876

Wadhawan, S. K. (2020). Late Quaternary Evolution of Clustered Parabolic Megadunes in Thar Desert, India. In *Quaternary Deserts and Climatic Change* (pp. 185-195). Boca Raton, FL: CRC Press. https://doi.org/10.1201/9781003077862-19

Wasson, R. J., & Hyde, R. (1983). Factors Determining Desert Dune Type. *Nature, 304,* 337-339. https://doi.org/10.1038/304337a0

Zhang, D., Narteau, C., & Rozier, O. (2010). Morphodynamics of Barchan and Transverse Dunes Using a Cellular Automaton Model. *Journal of Geophysical Research, 115,* F03041. https://doi.org/10.1029/2009JF001620

Zimbelman, J. R., Williams, S. H., & Johnston, A. K. (2012). Cross-Sectional Profiles of Sand Ripples, Megaripples, and Dunes: A Method for Discriminating between Formational Mechanisms. *Earth Surface Processes and Landforms, 37,* 1120-1125. https://doi.org/10.1002/esp.3243